Ince, E. S., Pagiatakis, S. (2017): GOCE Gradiometer Measurements Response to Ionospheric Dynamics. - *Journal of Geophysical Research*, *122*, 10, pp. 10712—10726.

DOI: http://doi.org/10.1002/2017JA023890

AGU PUBLICATIONS

JGR

Journal of Geophysical Research: Space Physics

RESEARCH ARTICLE

10.1002/2017JA023890

GOCE Gradiometer Measurements Response to Ionospheric Dynamics

E. Sinem Ince[1,2] **and Spiros D. Pagiatakis**[1]

[1]Department of Earth and Space Science and Engineering, Lassonde School of Engineering, York University, Toronto, Ontario, Canada, [2]Helmholtz Centre Potsdam, GFZ German Research Centre for Geosciences, Potsdam, Germany

Key Points:
- Equivalent ionospheric currents and GOCE-retrieved neutral winds in east-west direction are remarkably coherent
- GOCE measurement errors are modeled using external data that are markers of ionospheric dynamics
- Low Earth orbiter accelerometer measurements can be extensively used to investigate specific features over specific areas in space physics

Supporting Information:
- Supporting Information S1

Correspondence to:
E. Sinem Ince,
elmas.sinem.ince@gfz-potsdam.de

Citation:
Ince, E. S., & Pagiatakis, S. D. (2017). GOCE gradiometer measurements response to ionospheric dynamics. *Journal Geophysics Research: Space Physics*, *122*, 10,712–10,726. https://doi.org/10.1002/2017JA023890

Received 15 JAN 2017
Accepted 27 AUG 2017
Accepted article online 30 AUG 2017
Published online 25 OCT 2017

Abstract With the launch of dedicated satellite gravity missions, starting with CHAllenging Minisatellite Payload (CHAMP) in 2000, with Gravity Recovery and Climate Experiment (GRACE) in 2002, and Gravity field and steady-state Ocean Circulation Explorer (GOCE) in 2009, the accuracy and spatial resolution of the Earth's global gravity field models have been improved. Highly sensitive accelerometer measurements have not only been useful for gravity field modeling but have also been contributing to the studies of thermospheric dynamics. While improving the sensitivity of the accelerometer measurements, the new instrumentation used on board GOCE brings different challenges in understanding the data and developing sophisticated data processing. Our analyses reveal that the GOCE gravitational gradient measurements were affected by highly variable ionospheric dynamics that did not only degrade the quality of the GOCE Electrostatic Gravity Gradiometer (EGG) measurements but also proved that some characteristics of ionospheric dynamics can be measured by GOCE accelerometers and other Low Earth Orbiters. In this paper, we show how GOCE-retrieved neutral winds respond to main ionospheric currents and we develop the impulse-response relation between intense ionospheric dynamics (plasma drift) represented by Poynting energy flux and the gravity gradiometer tensor trace disturbances observed over the north geomagnetic polar region.

Plain Language Summary The European Space Agency's (ESA) GOCE satellite gravity mission was launched in 2009 to study the Earth's gravitational field with the help of a gradiometer and a GPS receiver mounted onboard. The gradiometer consisted of six accelerometers in a special configuration that measured gravitational and nongravitational accelerations in space. The quality of the GOCE accelerometer measurements was degraded over the Earth's polar regions during periods of increased solar activity that caused uncommon dynamics in the space environment, known as magnetic storms. This finding did not only require to reinvestigate the GOCE data processing but has also compelled scientists to use GOCE accelerometer measurements, in an inverse mode, to understand the Earth's upper atmosphere dynamics. In our recent contribution, we showed for the first time that there exists a direct relationship between GOCE gradient disturbances and magnetic storms over the Earth's polar regions. This contribution takes our previous findings a step further by developing a mathematical model that reduces the GOCE gradient disturbances up to 30% over North America and Greenland, using electromagnetic energy flow derived from terrestrial magnetic disturbance measurements. Our contribution paves the way for a combination of gravity and ESA's Swarm mission to study and understand the Earth's upper atmosphere physics.

1. Introduction and Background

The Gravity field and steady-state Ocean Circulation Explorer (GOCE) measured gravitational and nongravitational accelerations in three directions along its orbit at an altitude of about 260 km. The GOCE accelerometer measurements made possible for the first time the estimation of the second spatial derivatives of the Earth's gravitational potential from space. The latest version of the GOCE products of Level 1b processor version 5.06 has provided very high quality scientific data not only for geodesy, solid Earth, and oceanography (Drinkwater et al., 2006; Floberghagen et al., 2011; Rummel et al., 2011; Stummer et al., 2012) but also for the retrieval of thermospheric air density and thermospheric neutral winds and validation of thermospheric models (Bruinsma et al., 2014; Doornbos et al., 2013, 2014). Air density and neutral wind velocity retrieved from GOCE accelerometer measurements are used to study global ionospheric and thermospheric response

to geomagnetic storms (Lu et al., 2014), the vertical coupling between thermospheric layers (Gasperini et al., 2015), medium-scale gravity waves in the thermosphere (Garcia et al., 2016), and to observe wind jets and seasonal variations in the *F* region during "quiet times" (Liu et al., 2016). Moreover, there are numerous recent publications that use GOCE-derived thermospheric neutral winds also referred in the literature as "crosswinds" and air density profiles for further understanding of thermospheric-ionospheric studies as well as for model evaluation and assessment purposes (Doornbos et al., 2013; Drob et al., 2015; Lu et al., 2014). For the density retrieval and cross-track neutral winds derived from previous dedicated gravity missions, namely CHAllenging Minisatellite Payload (CHAMP) and Gravity Recovery and Climate Experiment (GRACE), the reader is referred to Bruinsma and Biancale (2003), Bruinsma et al. (2006), Doornbos et al. (2010), Forbes et al. (2005), Förster et al. (2008), Huang et al. (2016), Lühr et al. (2007), and Sutton et al. (2007).

GOCE was a geodetic mission and its ultimate goal was to develop accurate global gravity field models. Our previous studies investigated unknown signatures on the GOCE gravity gradiometer tensor (GGT) over the geomagnetic polar regions (Ince & Pagiatakis, 2016) that were speculated to be due to thermospheric cross-winds (Bouman et al., 2011, 2014; Brieden & Müller, 2014; Peterseim et al., 2011; Siemes et al., 2012; Stummer et al., 2012). These signatures appeared as disturbances in the GGT components of duration of 1–5 min, which may have leaked in the lower frequency part of the gradiometer measurement bandwidth (e.g., 60–200 s) (Ince & Pagiatakis, 2016). We showed that the disturbances on the GGT were internally consistent with the other GOCE Level-1b data (Frommknecht et al., 2011; Stummer et al., 2012), typically about 3–5 times larger than the expected measurement noise. Additionally, using data external to GOCE, we discovered an apparent relationship of the GGT disturbance groups with increased solar activity observed in the interplanetary magnetic and electric field data from the Advanced Composition Explorer (ACE) and Global Geospace Science Wind solar satellites and Poynting energy flux that was derived from the Equivalent Ionospheric Currents (EIC) and Spherical Elementary Current (SEC) amplitudes over North America and Greenland (Ince & Pagiatakis, 2016).

The impact of this discovery (Ince & Pagiatakis, 2016) is twofold. First, we showed that there is a causality of the GGT disturbances and energy input into the satellite environment, and this causal relationship can further be used to understand and subsequently model the GGT disturbances to improve the quality of GOCE and other follow-on Low Earth Orbiter (LEO) missions gravitational models. Second, our results showed that LEO accelerometer measurements provide very useful information about the main characteristics of the ionosphere and its dynamics, e.g., neutral winds, air density, and electromagnetic energy flux. This is consistent with Kelley et al. (1991), who showed conceptually that the electromagnetic energy flux into the atmosphere can reliably be measured remotely by polar-orbiting spacecraft at altitudes in the range of 400–1000 km using complete determination of the vertical component of the Poynting flux. In another publication, Fremouw et al. (1985) demonstrated with two examples that the Poynting flux can be estimated using measurements from the High Latitude Research Satellite (HiLat) spacecraft. In fact, even in the early 1960s, Feynman et al. (1964) discussed that the electromagnetic energy flow for steady or DC electric and magnetic fields can be conceptually measured by the Poynting energy flux.

In a more recent publication, Stolle et al. (2013) pointed out that enhanced solar wind and solar radiation energy input into near-Earth space result in strong electric currents flowing in the magnetosphere and ionosphere with significant plasma density structuring of neutral composition, and winds in the upper atmosphere. Such periods of enhanced activity cause rapid variations in the geomagnetic field of up to several hundred nanotesla within a few minutes and are called magnetic storms. Knipp et al. (2011) showed that during such geomagnetic field disturbances, there is generally increased Poynting flux at LEO altitudes; and moreover, large dayside Poynting flux events are important in magnetopshere-ionosphere-thermosphere coupling. Related to geomagnetic storms and Poynting flux, Huang et al. (2016) investigated the importance of Poynting flux in understanding the coupling process of ionosphere-thermosphere system and performed comparisons with GRACE- and GOCE-retrieved neutral winds during three different storm times.

In Peterseim et al. (2011), Stummer et al. (2012), and Siemes (2012), it is mentioned that the GGT disturbances over auroral ovals were due to crosswinds; however, no proof analyses were provided. Lack of proof may be due the fact that there were no actual neutral wind measurements available that could be compared to the GOCE GGT disturbances along the GOCE orbit for long periods of time. Peterseim et al. (2011) showed that these disturbances cannot be explained by scale factor adjustment and thus the cause of perturbations

remained unexplained until Ince and Pagiatakis (2016) showed that the GGT disturbances are coherent with the electromagnetic energy flow in the ionosphere. Recently, Siemes (2017) showed that the perturbations in the residual V_{yy} component can be accurately modeled by parameterizing the common mode accelerations in the cross-track direction multiplied by an unknown quadratic factor (Siemes, 2017, equation (50)). The quadratic factor was in fact nullified by measurements and adjustment of the position of the accelerometer proof mass during flight, and thus, it is surprising how a quadratic factor can explain such disturbances. Equation (50) (Siemes, 2017) shows that Siemes' approach is purely mathematical since it relates functionally the residual gradient V_{yy} with the common mode accelerations through the quadratic factor that inevitably absorbs most of the disturbances. Both V_{yy} and common mode accelerations are derived from the same set of fundamental measurements of accelerations.

In our recent studies (Ince & Pagiatakis, 2015, 2016), we showed that the ionospheric dynamics driven by electromagnetic energy flow (plasma drift or flow) is the dominating factor for the disturbances in the gravitational gradients but primarily in the cross-track direction. We emphasized that by reason of fundamental physical processes in the thermosphere at high latitudes, strong electric fields generated from the interaction between the solar wind and the Earth's magnetosphere cause electromagnetic energy flow that is fully described by the Poynting energy flux ($\vec{H} \times \vec{B}$, plasma drift; see next section). The Poynting flux derived from EIC and SEC has physical meaning and was used to further investigate the disturbances in the GOCE GGT. We introduced EIC and SEC (Weygand et al., 2011) derived from the magnetic field activity measured at terrestrial stations via the spherical elementary current systems (SECS) technique (Amm, 1997; Amm & Viljanen, 1999). Then, we used the EIC and SEC to calculate the Poynting vector (S vector) over North America and Greenland and performed coherency analyses of $\vec{S}$ with the GGT trace using continuous wavelet transform, wavelet coherence, and phase analysis of the cross wavelet spectrogram.

We thoroughly analyzed nearly 1000 ascending tracks during March–April 2011 when many minor to moderate magnetic storms occurred (Ince & Pagiatakis, 2016). About 100 of these tracks over Canada, Greenland, and surrounding oceans showed GGT disturbances of very specific structure and increased magnitude. Such disturbances in the gravitational gradients are at ~13 dB signal-to-noise ratio with respect to other sources that are within the noise level of the instrument. We proved that these GGT disturbances were highly coherent in time and space with electromagnetic energy flow input (Poynting flux) to the satellite environment (Ince & Pagiatakis, 2016). This was an important discovery, consistent with theoretical atmospheric physics principles leading to the modeling of the disturbances developed in this paper.

Defence Meteorological Satellite Program (DMSP)-derived Poynting flux might also have been used in this study, but the analyses could have been only performed over a very limited area, along the overlapping ground tracks of GOCE and DMSP satellites or on the long-term averaged characteristics. Therefore, we instead used EIC and SEC grids provided over Canada for every 10 s interval. Weygand and Wing (2016) investigated the current sheets connecting the Earth's magnetosphere to the Earth's high-latitude ionosphere that is derived from the DMSP satellites and SECS method. They found that the ionospheric current boundaries derived from the two are in agreement within 0.2° ± 1.3°, and the boundaries of these particular regions (accordingly, main currents) can be derived from terrestrial magnetometer observations which support our choice of data sets used in this study. In addition, we juxtapose the EIC and SEC with GOCE-retrieved horizontal neutral winds derived by Doornbos et al. (2013) to conclude that using EIC and SEC is necessary and sufficient to further investigate and model the GGT disturbances.

In this contribution, we first describe the data sets used and concentrate on an example encompassing five successive tracks over Canada and Greenland during a geomagnetically active period. We present the EIC and SEC values as well as GOCE-retrieved neutral wind profiles computed by Doornbos et al. (2013) along these five tracks. In these examples, we show that the eastern, northern, and upward components of the neutral wind velocity retrieved from the GOCE accelerometer measurements exhibit similar characteristics, as it should, to the principal ionospheric currents represented by EIC and SEC, particularly showing increased wind speeds during elevated electromagnetic storms.

Consequently, we make the hypothesis that the disturbances are mainly driven by EIC and SEC, which we subsequently use to derive "equivalent" Poynting energy flux in the north-south and east-west directions of the satellite track. The Poynting energy flux is then used as input (driving force) into the satellite environment to derive the response of GGT to this energy flow increase that induces the disturbances. In other words, we assume that the Poynting energy flux is the fundamental and physically meaningful driving force to model

the GGT disturbances rather than the thermospheric neutral winds which are principally driven by the electromagnetic energy flux in the thermosphere. Besides, thermospheric neutral winds from external sources, except interpolated values from low spatial and temporal resolution models, are in fact not available along the GOCE tracks.

Later in this contribution, using a data-driven autoregressive exogeneous model, we develop the relationship between the disturbances observed in the GGT tensor trace and the plasma drift, the latter being represented by the Poynting energy flux. Then, we use this model to predict the disturbances and correct the original GGT trace over Canada and Greenland along all ascending tracks. Not only is this study important for bridging geodesy and space physics/ionospheric dynamics but also it is crucial for studying the response of crosswinds to ionospheric currents, improving the quality of GOCE Electrostatic Gravity Gradiometer (EGG) products, and establishing how ionospheric dynamics affect the low Earth orbiters.

2. Data and Preanalyses

The data sets we use in this research consist of GGT diagonal elements that are filtered into the GOCE gradiometer measurement bandwidth (MBW), [10–200] s, and into [180–300] s, a bandwidth which includes lower frequency components than the GOCE EGG MBW, and GGT trace that is retrieved from the filtered diagonal GGT gradients in [180–300] s. In addition, we use northward, eastward, and upward components of wind velocity (Doornbos et al., 2013), Equivalent Ionospheric Currents (EIC) and Spherical Elementary Current (SEC) amplitudes (Weygand et al., 2011), and finally Poynting vector components that are calculated from the EIC and SEC (Ince & Pagiatakis, 2016). The GGT trace and the EIC, SEC, and Poynting flux that are computed from terrestrial magnetometer measurements have different spatiotemporal resolutions, and preprocessing is required to perform coherency analyses with the GGT trace.

The preprocessing of the data sets is given in this section, and the following data sets are retrieved:

1. The diagonal GGT components filtered into the gradiometer MBW, [10-200]s and the trace as the summation of the filtered diagonal components.
2. The diagonal GGT components filtered into the lower frequency band, [180–300] s, and the trace as the summation of the filtered diagonal components.
3. The northward, eastward, and upward components of the wind velocity retrieved from GOCE accelerometer measurements along the satellite track and decimated into 10 s interval (wind speeds are computed by E. Doornbos and downloaded from ESA's Virtual Archive at https://earth.esa.int/web/guest/-/goce-data-access-7219).
4. EIC and SEC values interpolated into the satellite position by using the gridded EIC and SEC data given in 10 s temporal resolution (grid values are computed and published by J. Weygand at http://www.igpp.ucla.edu/jweygand/htmls/EICS_NA_Greenland.html).
5. Poynting vector computed from EIC and SEC that is interpolated into the satellite position. Consequently, the Poynting vector is transformed into the Gradiometer Reference Frame (GRF) along the satellite track using inertial attitude quaternions and Earth orientation parameters.

2.1. GOCE Measurements

2.1.1. Gravitational Gradients and GGT Trace

In order to understand the characteristics of the Gravitational Gradient Tensor (GGT) disturbances, we extend our study to the individual diagonal gradients. For the methodology of GOCE data processing, the reader is referred to Floberghagen et al. (2011), Frommknecht et al. (2011), Rummel et al. (2011), and Stummer et al. (2012). In this contribution, we initially compare the cross-track component of the GGT V_{yy} with that computed from ITSG-Grace2014k (Mayer-Gürr et al., 2014) geopotential model at the satellite altitude.

First, GRACE model-based gradients are calculated at the satellite altitude from spherical harmonic coefficients up to degree and order 200 using the software provided by the Technical University of Munich (T. Gruber, personal communication, 2016). Then, each gravitational gradient is transformed into the GRF (ESA, 2006) and band-pass filtered into the EGG measurement bandwidth (MBW), [10–200] s. The MBW-filtered GOCE EGG gravitational gradients are compared with the MBW-filtered ITSG-Grace2014k based series, and their differences along ascending tracks are geographically presented in Figure 1a, whereas Figure 1b shows the trace corresponding to the same epochs as in Figure 1a. Note the similarity of the signatures in the two figures over the geomagnetic polar regions, whereas the trace (Figure 1b) shows noisier characteristics globally.

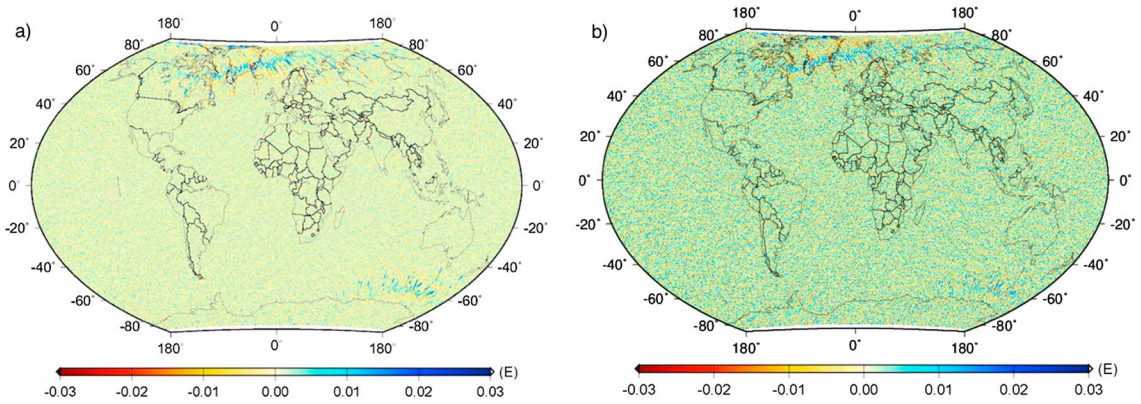

Figure 1. (a) The GOCE EGG measured V_{yy} is compared with the ITSG-Grace2014k model (D/O 200) computed gradients within the EGG MBW during March–April 2011 for ascending tracks. The difference between them indicates unknown discrepancies over the geomagnetic polar regions. (b) The trace of the GGT obtained from the filtered diagonal GGT components within the EGG MBW. Note the similarity between the two signatures over the geomagnetic polar regions.

Our analysis and results show that the differences between the GOCE V_{yy} and model computed V_{yy} can exceed 30 mE over the geomagnetic polar regions (see also Siemes, 2012; Stummer et al., 2012; Peterseim et al., 2011) within the MBW. For the interested readers, it is worth mentioning that the comparison results of V_{xx} and V_{zz} do not show similar high level noise over the polar regions (see also supporting information Figures S1–S2). This proves that there are substantial discrepancies between the GOCE EGG measurements and model-computed V_{yy}, and this is an additional verification of the errors present in the GOCE EGG V_{yy}.

2.1.2. Thermospheric Neutral Winds

As mentioned in section 1, the GOCE accelerometer measurements together with thruster data have been used to retrieve the northward, eastward, and upward components of the neutral wind velocity. Due to the limitations in the measurement process, it is not possible to retrieve the full wind vector (Doornbos et al., 2014) and the along-track wind speed is realized from a model value, whereas the vertical component is assumed to be zero while computing the horizontal wind speeds. Therefore, the neutral wind velocity that is provided in a reference frame with components in the eastward (zonal), northward (meridional), and upward (vertical) directions should not be interpreted as the full zonal (eastward) or meridional (northward) winds. The reader is referred to Doornbos et al. (2013) and Doornbos et al. (2014) for the details of the methodology.

In this contribution, time series of the components of neutral wind velocity are used for comparison purposes with EIC and SEC along five satellite tracks shown in Figure 2. The five tracks on 1–2 April 2011 starting at 19:42, 21:12, 22:42, 00:11, and 01:41 UTC are presented. Since we investigate the GGT unknown signatures over the North geomagnetic polar region, we perform our analyses on the GOCE-retrieved crosswinds over this limited area between latitudes 30°N and 90°N as well. The northward, eastward, and upward components of the wind velocity are presented in Figures 3a–3c, respectively, where the different tracks are represented by different colors.

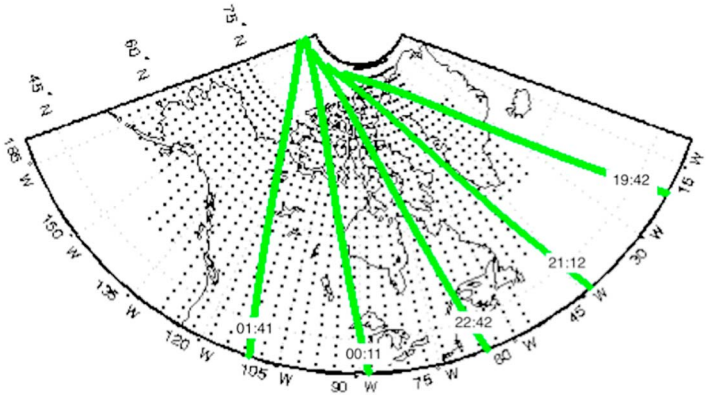

Figure 2. The five successive tracks over Canada and Greenland are used to investigate the relationship between neutral winds and equivalent ionospheric currents. Track starting times (UTC) are indicated on each track.

The wind components in all three directions show similar along-track structure in all five tracks with a visible phase shift. This shift is due to the use of geographical coordinates used (instead of geomagnetic coordinates) in this representation as well as to the structure of the signatures distributed over the auroral oval. The eastward wind component (Figure 3b) exhibits significant variations over the latitudes between 50°N and 75°N (see also supporting information Figure S3 for the representation wrt geomagnetic coordinates). Similar variations are observed in northward and upward components as well, whereas the upward component is much smaller than the other two; note that in Figure 3c, the vertical scale is 100 times smaller than in Figures 3a and 3b. Their comparisons to main ionospheric currents are given in the next section.

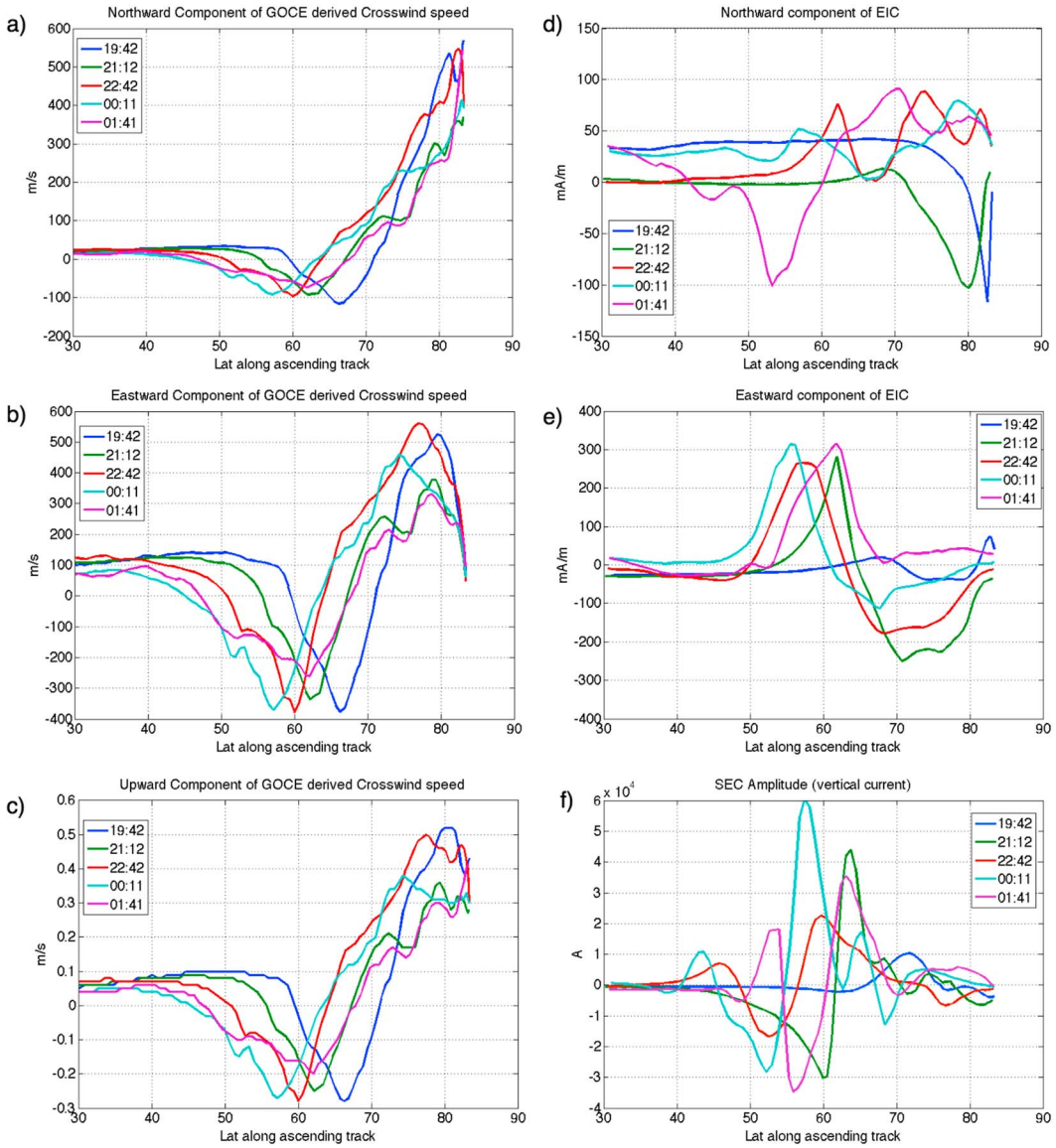

Figure 3. Crosswind speed derived from GOCE accelerometer measurements and thruster data and corresponding EIC and vertical currents along the five successive tracks. (a) Northward component of the crosswind speed. (b) Eastward component of the crosswind speed. (c) Upward component of the crosswind speed. (d) Northward component of horizontal EIC. (e) Eastward component of horizontal EIC. (f) SEC amplitude (vertical current).

2.2. Ionospheric Electrical Currents

Complex electrical current systems are represented by a simple set of equivalent electrical currents at a specific altitude in the ionosphere by using the Spherical Elementary Current Systems (SECS) method (Amm, 1997). In this study, we use Equivalent Ionospheric Current (EIC) and Spherical Elementary Current (SEC) amplitudes derived from terrestrial observatories over North America and Greenland (Weygand et al., 2011). Computed current values are provided on a grid at 10 s temporal resolution, whereas the terrestrial stations have ~350 km spatial resolution in the densest regions in Alaska (Weygand et al., 2011).

EIC in the north-south and east-west directions is given in mA/m, whereas SEC vertical currents in upward and downward directions are given in Amperes, in a left-handed local coordinate system. The EIC and SEC do not share the same grid area and resolution. We apply the collocation method (kriging) to interpolate the grid values into the satellite ground track positions for coherency analysis. In Figures 3d–3f, we present the northward and eastward equivalent ionospheric current components and vertical currents, respectively. Since we investigate the variations of the currents, we did not transform them into the GRF at this stage.

The northward EIC component shows complicated and inconsistent behavior among the five tracks. This might be due to the rapid changes in the thermosphere in the north-south direction along the satellite track. On the contrary, the eastward component shows consistency and similarities in all five tracks when the ionosphere was geomagnetically active. The phase delay between the signatures over the five tracks is again due to the chosen geographical coordinate system as well as due to the nature of the signatures. One can easily notice the coherency between the eastward components of the neutral winds (crosswind) and the EIC. Therefore, this coherency is commensurate with the theory that neutral winds are driven, enhanced, or highly modified by ionospheric currents at auroral ovals.

It is worth mentioning that at high latitudes, thermospheric neutral winds are driven by several sources, such as momentum exchange between convecting ions and the neutral gas (ion drag); solar heating produced pressure gradients, joule heating, and auroral particle precipitation; and inertial forces (e.g., Coriolis and centrifugal) (Kwak & Richmond, 2007). Also, it is given in Killeen and Roble (1993), Roble (1996), and Thayer and Killeen (1988) that the ionospheric plasma convection (plasma drift) can significantly modify the pressure gradient-driven neutral wind flow. Since an external neutral winds data set of high spatiotemporal resolution is not available along GOCE orbits, the high temporal resolution of EIC and SEC can be used for further studies over North America and Greenland. Besides the similarities between the behavior of the neutral winds and equivalent currents in the eastward direction, the well-structured anticoherence between them is worth investigating.

By visual inspection of Figure 3, there also exists correlation between the eastward wind speed and the vertical currents. SEC values (vertical currents) presented in Figure 3f are proportional to field-aligned currents for uniform conductance, and the relation between the SEC and the eastward component of GOCE-retrieved wind speed indicates that the current input to the ionosphere and drifting away from the ionosphere plays an important role on the behavior of the neutral winds.

Another significant finding relates to the dynamics of the ionosphere at different altitudes. The EIC and SEC values are provided at an altitude of 110 km where the main ionospheric currents are present. The neutral wind velocity components that are derived from GOCE accelerometer measurements are computed at altitude of approximately 250 km. The coherency between the EIC-SEC and GOCE-retrieved winds is striking, and investigations of other conditions and storm times are needed for further understanding. Huang et al. (2016) argue that the Poynting flux is the dominant form of energy input to the ionosphere-thermosphere system. Moreover, they indicate that any thermospheric response to a magnetic storm must involve energization of ions since neutral particles cannot be energized by the electromagnetic waves directly. Therefore, coupling of different layers still needs to be understood better. Huang et al. (2016) also show the comparison of neutral density estimations retrieved from GRACE and GOCE that is at different altitudes, 470 and 275 km, respectively. They found that the largest increases in neutral density at both altitudes occur at high latitudes as of our interest. Within the same topic, Lu et al. (2014) compared the Thermosphere Ionosphere Mesosphere Electrodynamics General Circulation Model (TIMEGCM) and GOCE- and CHAMP-retrieved thermospheric wind and density which reveals some differences between them. The TIMEGCM simulations underestimated neutral mass density in the upper thermosphere and overestimated the storm recovery time. They mentioned that these discrepancies indicate that the simulations do not fully represent some heating or circulation dynamics and potentially cooling processes, and also some parameterization updates to TIMEGCM are established.

Based on our investigations presented in Ince and Pagiatakis (2016) and analyses presented in this section, we use Poynting flux computed from EIC and SEC. The use of Poynting flux instead of equivalent currents is expected to provide physical meaning to our analyses. In section 3, we develop the data-driven relationship between the Poynting flux that represents the ionospheric dynamics (plasma drift) and the disturbances in the gradients. Understanding the variations due to the altitude change is beyond the scope of this contribution, and the reader is referred to Huang et al. (2016) for more details.

2.3. Poynting Energy Flux

We proceed to estimate the electromagnetic energy density flow (energy flux) using EIC and SEC amplitudes that are calculated on a spherical geographic grid. In order to compute the Poynting vector from EIC and SEC, EIC (mA/m) is assumed to represent horizontal magnetic field components, whereas the SEC (Amperes) is normalized by the area of the grid cells and represents the electric field current intensity per unit area (A/m^2) in upward (positive) and downward (negative) directions in a local coordinate system. The electromagnetic energy flow direction is represented by the Poynting vector.

The Poynting vector can be represented as

$$\mathbf{S} = \mathbf{E} \times \frac{\delta \mathbf{B}}{\mu_0}, \tag{1}$$

which is the cross product of the convection electric field, **E**, with the perturbation vector of the geomagnetic field $\delta\mathbf{B}$ with respect to the main geomagnetic field $\mathbf{B_0}$, and μ_0 is permeability (Kelley, 2009) and it is represented in units of J/sm^2 or W/m^2. In general, the direction of the Poynting vector (*S* vector) indicates the direction of the propagation or flow of electromagnetic energy that drives the ionospheric plasma drift. As presented in Figure 3, the variations of the neutral wind speed are highly coherent with the variations of ionospheric currents. Therefore, we can make the hypothesis that the direction and amplitude changes of the Poynting vector correlate with the drag in the satellite orbit and become the driving force of the disturbances observed in the GGT (Ince & Pagiatakis, 2016).

Because of the reasons mentioned in the previous section, we are motivated to compute the Poynting vector instead of using equivalent currents, which has a physical meaning and indicates the direction of the flow of electromagnetic energy and therefore the energy input to the satellite environment. It is worth noting that, for the sake of the correctness of our analyses, the Poynting vector computed from the EIC and normalized SEC is furthermore transformed into the GRF by using the azimuth angle of the satellite ground track with respect to the geographical north about the *Z* axis of the gradiometer. In the following section, the cross-track Poynting vector component is used for modeling purposes.

3. Methodology

3.1. Description of the Dynamic System

We use an input-output dynamic system approach according to which an input signal is introduced to a linear dynamic system and an output signal is produced based on the response of the system (impulse-response) as given in Figure 4. In parametric linear models, the input is related to the output in difference or differential form, which can be represented by Laplace or z-transform forms, whereas in nonparametric linear models, the system properties are represented by curves.

In our case, the very complex physics behind the way the disturbances are introduced into the EGG gradients is unknown and the system can only partly be understood based on the response analysis. In order to remove the disturbances, data-driven models are examined and used in this study. Unless otherwise indicated, the information on data-driven modeling presented in this section is taken from Andersson et al. (1998) and Lennart (1999).

3.2. Data-Driven Modeling

A dynamic system that processes an input signal to produce an output signal is designed according to the purpose it is intended to serve. In studying the GOCE GGT trace disturbances caused by intense ionospheric dynamics, the relationship between the input (cause) and output (effect) is not defined, or more precisely, it is not known. In such cases, it is possible that the input and output signals are measured. By using the measured input and output signals, modeling their unknown relationship (impulse response of the dynamic system) may be possible. The unknown relationship can be categorized using linear or nonlinear model structures. Even though it is very possible that we deal with a nonlinear system (e.g., NARX and NARMAX), in this example we rely on a linear model structure as an acceptable approach. Matlab System Identification Toolbox is used in the investigations (Lennart, 1999).

We develop this relationship (model) using the Poynting energy flux in the cross-track direction as the input to the system (GOCE) and the disturbances observed in the GGT trace as the output from the system (Ince & Pagiatakis, 2016). The methodology we apply here consists of various steps, such as preprocessing of the data, and estimation and validation of the model. As mentioned in the previous section, first the GGT diagonal elements are filtered into the frequency bandwidth of interest, [180–300] s and downsampled into 10 s interval, whereas the EIC and SEC are interpolated (using kriging) into the satellite position along the satellite track. The Poynting vector is computed based on the interpolated EIC and SEC values along the satellite track and transformed into the GRF later. Based on our analyses in different frequency bands, we conclude that the coherency between the disturbances and Poynting flux is higher and more robustly defined in the interval of [180–300] s. Therefore, further investigations are performed in this frequency band and not in the nominal bandwidth of the instrument [10–200] s. After preprocessing (e.g., detrending, filtering, resampling,

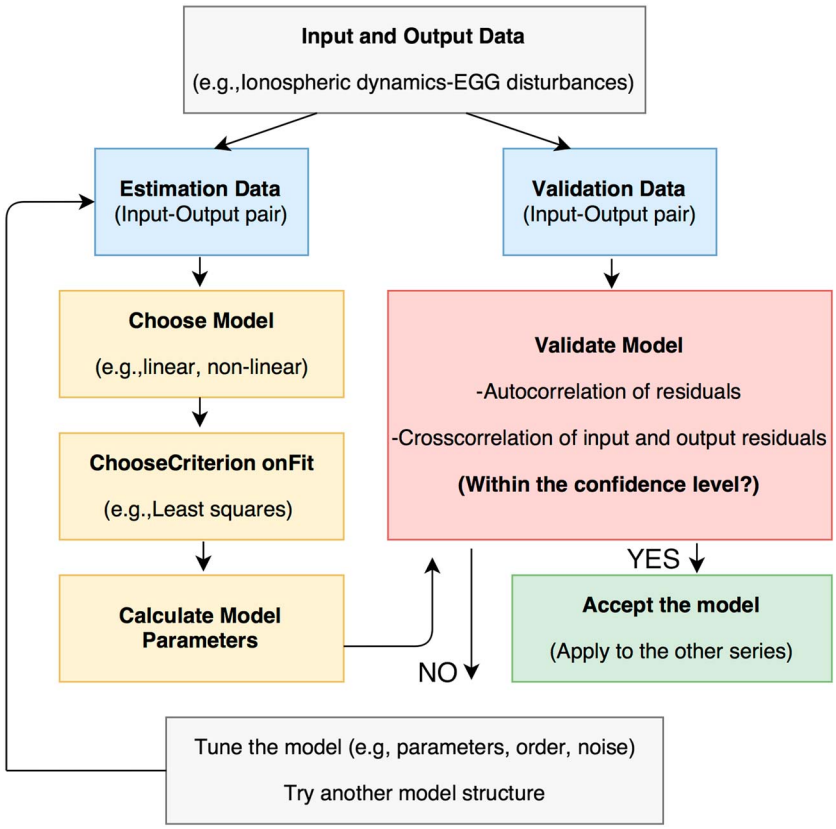

Figure 4. Input-output dynamic system representation.

and transformation), the data are analyzed into two separate stages, namely, the estimation and validation stage. Estimation data are used to develop the model, whereas the validation data are used to test the validity of the model by means of residual analyses.

The disturbances observed in GOCE EGG data are assumed to be coming from ionospheric dynamics, whereas calibration and instrumental errors, or errors in data processing are assumed as nonmeasured and are not considered in the model development but are part of the noise. In our case, we represent the relationship between the input and output signals by a linear (parametric/ nonparametric) model. Because GOCE gradiometer disturbances are not well-known nor have they been studied before, our initial solution is based on testing many input-output relations.

Once the model parameters are determined, the model is used to simulate the output signal which is then compared with the original (measured) output signal (validation stage). A least squares fit analysis is performed and the fitting is given in terms of percentage. In a second step, the residuals are analysed for the purpose of assessing the suitability of the model. Residual analyses are performed using the autocorrelation of the residuals themselves as well as the cross correlation of the input signal and the residuals (which ideally should be zero). When the correlation results show coefficients within the confidence level of 95%, then the model can be accepted as a successful and effective model for the intended application.

Based on the description and tests mentioned above, after testing many input-output pairs, we found that the Autoregressive Exogeneous Model (arx) of the order 6 is applied to our system with reasonable results. We did not characterize the type of the noise as it is the case for ARMAX model type. Instead, we assumed the noise to be white noise and considered an ARX model. The formulation of ARX model can be written as

$$y(t) + a_1 y(t-1) + \ldots + a_{na} y(t-na) = b_1 u(t-nk) + \ldots + b_{nb} u(t-nk-nb+1), \quad (2)$$

where $u(t)$ is the input to the system, $y(t)$ is the output from the system, a and b are polynomial coefficients, and nk is the input-output delay.

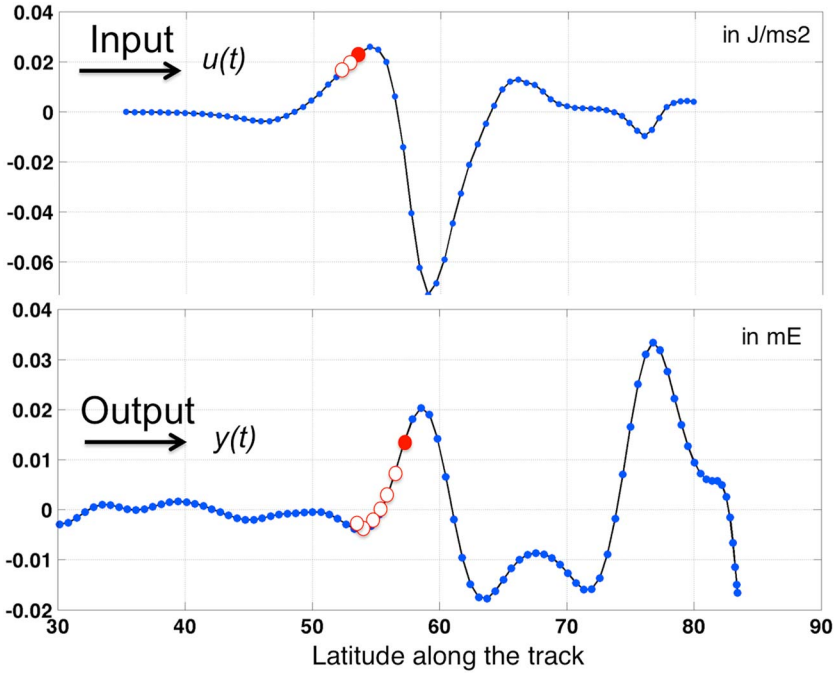

Figure 5. The depiction of the arx625 model. Note the 50 s delay between the solid red circles in the input and output signals which indicate the delay (lag) of the system response.

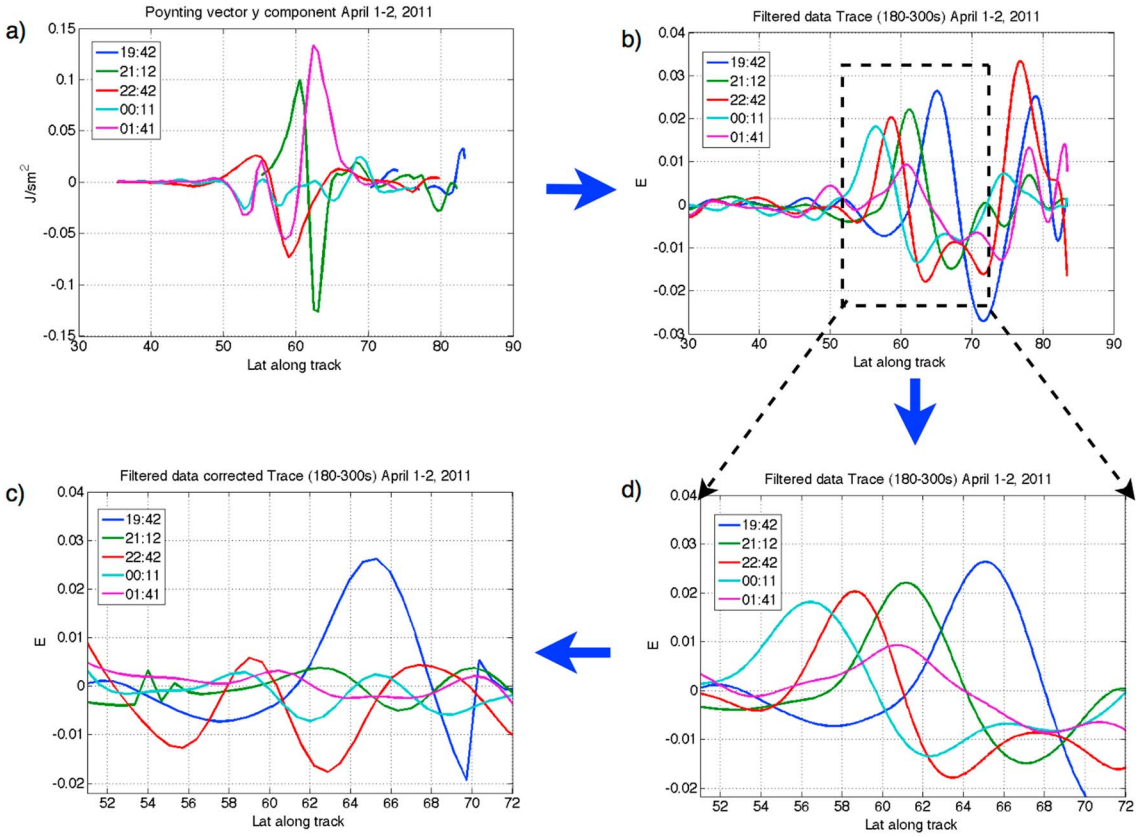

Figure 6. Five successive tracks each shifted by 15° in ascending node are investigated. (a) Poynting vector components in cross-track direction. (b) GOCE EGG trace. (c) Corrected trace after the data-driven model applied. Note the elimination of the disturbances, except the first track represented by blue color. (d) GOCE GGT disturbances within the area where the input signal was available. Note that the blue track crosses Greenland and shows a signature of the disturbance stating from latitude 60°N. The successive tracks cross 15° to the west of the previous track and experience similar signatures over similar regions with small phase differences.

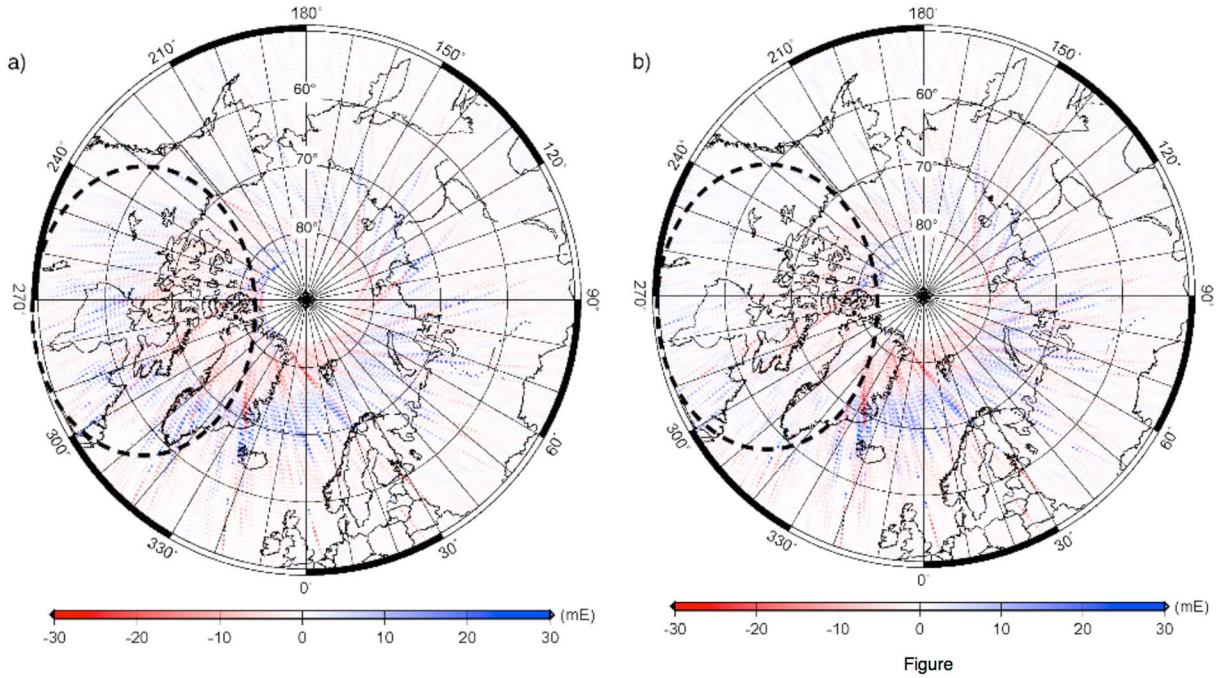

Figure 7. (a) Trace obtained from filtered diagonal gravity gradients downsampled in 10 s interval during March–April 2011. Note the signatures over high latitudes and auroral oval. (b) Corrected trace obtained by using model arx625 during March–April 2011. Note the improvement over Canada and western Greenland.

The arx625 model is described using real input and output signals referring to the latitude along the track in Figure 5. The input and output series are represented by $u(t)$ and $y(t)$, respectively. The model is named "arxnanbnk" (e.g., arx625 where $na = 6$, $nb = 2$, and $nk = 5$) where na is the number of poles, nb is the number of zeros, and nk is the delay (δ) or the number of samples (5 samples × 10 s = 50 s delay) before the input affects the system output, respectively.

The solid red circle in the output signal shows the epoch of the simulation. The preceding red circles (open) indicate measurements that are also taken into account in the model development. The solid red circle in the input signal indicates the epoch of the input signal that is used in the computations which corresponds to the epoch of simulation by a delay of five sample points. Moreover, the previous points marked in the input signal by open red circles indicate that there are effects also contributing to the output signal, originating from measurements collected at previous epochs.

4. Modeling the Disturbances

We investigated the trace of the five successive tracks as depicted in Figure 6. In these examples, the trace is retrieved as given in section 2. The five tracks with different colors cross Greenland and Canada within a few hours (see Figure 2). The cross-track Poynting vector components (input signal) are depicted in Figure 6a. The blue line represents a track over Greenland that has the Poynting vector component computed over an area with limited availability of EIC and SEC. The track shown in red crosses Labrador Sea and Davis Strait. Even though there are no actual measurements of geomagnetic disturbances performed over the seas, the measurements on land are used to recover the gridded ionospheric currents (Weygand et al., 2011) in these regions, and therefore, the geomagnetic disturbances are available for modeling. The red line shows distinctive variations that change to negative magnitudes at about latitude 55°N, which corresponds to the region where we observe distinctive trace disturbances.

The five GGT traces (output signal corresponding to the five tracks) are depicted in Figure 6b using the same color code as in Figure 6a. The disturbances show similar behavior between latitudes 60°N and 80°N. As the track shifts from east to the west, the disturbance signature also displaces slightly to the south. For example, the track starting from 19:42 UTC on 1 April, as shown in blue, depicts the variation starting from latitude

Table 1
Statistics of 954 Ascending Tracks Before and After Corrections Based On Arx625 Transfer Function

Trace	30–87°	50–85°	50–60°	50–70°	60–70°	60–85°
Std	2.7 (2.3)	3.2 (2.6)	1.5 (1.4)	2.7 (2.2)	3.1 (2.5)	3.6 (2.9)

Note. See the values in parenthesis for the statistics of corrected series. The values are given in mE.

62°N which returns to its normal structure over latitude 82°N. The next ground track shown in green over a different region starting at 21:12 UTC time experiences similar effects as the previous track, but at different geographical latitudes.

Figure 6d shows the measurements along the five tracks focusing on the interval between latitudes 50°N and 72°N where the Poynting vector is available. The developed model is applied to the trace, and the corrected trace is presented in Figure 6c. Except the blue line, the trace in the other four tracks shows significantly reduced effects. The average RMS improvement in the five tracks is over 30% (nearly 10 dB) between latitudes 50°N and 70°N. The disturbance observed in the trace starting at 19:42 UTC (blue) is not eliminated because the track is located over the ocean and partly over Greenland; the Poynting vector components (input) are not available at the epochs corresponding to disturbed tracks. Therefore, not all large signatures are removed from the trace in the areas that are outside of the gridded EIC and SEC presented in Ince and Pagiatakis (2016) and Weygand et al. (2011).

The trace that is obtained from the filtered diagonal gradients for the 2 month period is displayed in Figure 7a. The GGT disturbance signatures over the auroral oval are distinguishable and similar to the ones displayed in Figure 1. The corrected trace over Canada and Greenland is shown in Figure 7b for the same time period, March–April 2011. The reduced signatures over the Hudson Bay in Canada and western Greenland shown in the black circle are very distinguishable and now within the noise level of the instrument. The overall RMS improvement is about 20%. Consequently, we can say that the methodology we use here is successful but, as expected, is limited by the spatial availability of the EIC and SEC (Poynting vector).

The statistics of the original filtered trace and corrected trace are given in Tables 1 and 2 for 954 tracks during March–April 2011 and the five tracks presented, respectively. The standard deviations are presented for different latitude bands over the high latitudes. The standard deviation is computed for each track (954 in total and 5 for the tracks shown in the example), and the average value is given in the tables. The statistics of the corrected series are given in parenthesis. The six different latitude intervals are, namely, 30–87°N, 50–85°N, 50–60°N, 50–70°N, 60–70°N, and 60–85°N, and the statistics are calculated for ascending tracks only. It is also worth noting that the statistics of 954 tracks do not only represent the statistics of disturbed tracks but also the ones that are within the noise level of the instrument. However, the five tracks we look into are all noisy tracks, and their statistics should be able to represent the improvement of the corrections better.

Table 2 shows the statistics of the five disturbed tracks for the six latitude bands. It is found that the largest disturbances occur over the latitude band 60–85°. It is critical that the higher altitudes show higher standard deviations which also indicate the more intense dynamics in these regions. We find that 20–30% improvement has been accomplished after the corrections applied. It is worth mentioning that the latitude band 50° to 70° shows the largest improvement. This improvement is probably due to the high availability of the input data (Poynting vector) over this band.

Table 2
Statistics of the Five Ascending Tracks Before and After Corrections Based On Arx625 Transfer Function

Trace	30–87°	50–85°	50–60°	50–70°	60–70°	60–85°
Std	8.4 (6.7)	10.2 (7.5)	6.3 (4.5)	9.9 (6.8)	9.0 (6.5)	11.0 (8.1)

Note. See the values in parenthesis for the statistics of corrected series. The values are given in mE.

5. Discussion and Conclusions

In this contribution, we studied and modeled the disturbances of high-resolution GOCE gravitational gradients using atmospheric physics. We showed that the disturbances occur both in the north and south magnetic polar regions with different characteristics and may reach up to a few to several times the noise level of the instrument (∼11 mE). To understand the source of these disturbances, we used external data sets to GOCE, namely, equivalent ionospheric currents and vertical current amplitudes which were shown to be consistent with the GOCE-retrieved neutral winds. We showed that the eastward component of the neutral wind velocity supports the hypothesis of using electrical currents in the ionosphere to understand and investigate the EGG disturbances further over this particular area since the interactions between the two are rapid. This finding also establishes that the GOCE accelerometers measured the variations that were due to the ionospheric plasma flow and the features of its consequences. Our contribution is entirely based on the physics of the ionospheric dynamics and on independent measurements thereof, as opposed to the pure mathematical approach developed by Siemes (2017).

Another finding is that the equivalent ionospheric currents that are computed at an altitude of 110 km have similar structure to the GOCE accelerometer-retrieved eastward neutral wind component at an altitude of 250 km. This might be a consequence of the similarities in the "main" characteristics of neutral winds at different altitudes over high-latitude areas.

With the evidence that the EIC and SEC can further be used in understanding GOCE disturbances, we developed a model driven by ionospheric dynamics represented by Poynting energy flux. In other words, we developed a model based on the ionospheric dynamics and GOCE GGT disturbances as an impulse-response model making the hypothesis that the ionospheric dynamics as a whole were the dominating cause of the GGT disturbances. This hypothesis is physically valid because the EIC and SEC describe, by definition, equivalently the total ionospheric dynamics regime. Equivalent ionospheric currents are a good approximation of the currents describing the spatial and temporal varying behavior of the fundamental processes in the ionosphere (Untiedt & Baumjohann, 1993; Zhang et al., 2013). The developed model was validated using a different set of input-output series and consequently applied to correct the disturbances over the regions where Poynting energy flux was available. We demonstrated for the first time that the disturbances observed in GOCE GGT trace can be reduced/eliminated based on the limited information retrieved from EIC and SEC. Moreover, following the work done on the air density enhancement retrieved from CHAMP accelerometer measurements and their comparisons with ionospheric dynamics by Lühr et al. (2004), we demonstrated that there is a direct relation between the acceleration measurements in space and the variations caused by the increase of the electromagnetic energy flow.

In order to extend the area of improved gradients, the EIC and SEC amplitudes over Scandinavia and Russia need to be included in further investigations and modeling. Our analyses considered the development of a corrective model over North America and Greenland, and this was limited by the availability of the EIC and SEC. Similar models over the South Pole can be used to improve the data in that region. Accordingly, we conclude that the static geopotential models over the geomagnetic polar regions can still be improved with the contribution of enhanced GOCE EGG products. By further improving the GOCE data processing, detecting and monitoring the time-variable Greenland gravity field may be improved (Bouman et al., 2014) which is also crucial for sea level variation studies. Our on-going analyses include investigations on V_{yy} component, particularly with enhanced analyses in different frequency bands. The outcome of this research may help reduce the disturbances and improve the EGG products and accordingly contribute to gravitational field modeling as well as to ionospheric-thermospheric modeling via the measurements of nongravitational accelerations.

We emphasize that GOCE was not only a very successful geodetic mission but also very useful for space weather studies (e.g., detection of gravity waves and retrieval of thermospheric winds, comparisons with wind models) as shown by Bruinsma et al. (2014), Doornbos et al. (2013), Drob et al. (2015), and Lu et al. (2014). GOCE accelerometer measurements can furthermore be used to understand the ionospheric dynamics and evaluate the equivalent ionospheric currents derived from terrestrial observations and help estimate the currents (e.g., EIC and SEC) where no magnetometer measurements exist or help evaluate them at different altitudes.

While our contribution is limited to North America due to lack of geomagnetic observations globally, it provides important scientific basis for upcoming LEO missions, such as GRACE Follow-on, and their integration with Swarm. Swarm provides global geomagnetic field and electric currents flowing in the magnetosphere

and ionosphere; ionospheric density and flow; and temperatures and other parameters, as well as their temporal variations (e.g., Knudsen et al., 2017). The integration of follow-on LEO gravity missions with Swarm will lead to a global and comprehensive study and modeling of the accelerometer and orbit disturbances better that will improve the gravity geopotential models (direct mode), whereas at the same time the inverse modeling will provide additional information from LEO gravity missions to ionosphere modelers.

In summary, the idea to study the extent to which GOCE gradiometer measurements and specifically their disturbances can provide information about the electromagnetic field is fundamental for trans-disciplinary research. This is possible via the integration of geodetic LEO missions with Swarm and other upcoming space missions. Lastly, providing redundant and independent measurements when studying the ionospheric dynamics and space weather is essential for understanding the Earth system and, in particular, the Geospace.

Acknowledgments
This research was supported by the Natural Sciences and Engineering Research Council of Canada (NSERC) discovery grant and Carbon Management Canada. GOCE electrostatic gravity gradiometer data are provided by European Space Agency, and GOCE crosswind data were computed by Eelco Doornbos. Both data sets are downloaded from ESA's Virtual Online Archive. James Weygand of the University of California at Los Angeles is thanked for making EIC and SEC data publicly available and further discussions on the SECS method. GOCE team in Technical University of Munich is thanked for contributing in the computation of the V_{yy} from GRACE model. Lastly, ESA and GFZ section 1.2 scientists are thanked for supporting this research with their knowledge and very helpful discussions. Wind speeds are computed by E. Doornbos and downloaded from ESA's Virtual Archive at https://earth.esa.int/web/guest/-/goce-data-access-7219. EIC and SEC grid values are computed and published by J. Weygand at http://www.igpp.ucla.edu/jweygand/htmls/EICS_NA_Greenland.html).

References

Amm, O. (1997). Ionospheric elementary current systems in spherical coordinates and their application. *Journal of Geomagnetism and Geoelectricity*, *49*(7), 947–955.

Amm, O., & Viljanen, A. (1999). Ionospheric disturbance magnetic field continuation from the ground to the ionosphere using spherical elementary current systems. *Earth, Planets and Space*, *51*(6), 431–440.

Andersson, L., Jönsson, U., Johansson, K. H., & Bengtsson, J. (Eds.). (1998). A manual for system identification. *Laboratory Exercises in System Identification*, KF Sigma i Lund AB. Department of Automatic Control, Lund Institute of Technology, Box, 118, S-221 00: Lund, Sweden.

Bouman, J., Fiorot, S., Fuchs, M., Gruber, T., Schrama, E., Tscherning, C., … Visser, P. (2011). GOCE gravitational gradients along the orbit. *Journal of Geodesy*, *85*(11), 791–805.

Bouman, J., Fuchs, M., Ivins, E., Wal, W., Schrama, E., Visser, P., & Horwath, M. (2014). Antarctic outlet glacier mass change resolved at basin scale from satellite gravity gradiometry. *Geophysical Research Letters*, *41*(16), 5919–5926. https://doi.org/10.1002/2014GL060637

Brieden, P., & Müller, J. (Eds.). (2014). Cross-overs assess quality of GOCE gradients. *Observation of the System Earth from Space-CHAMP, GRACE, GOCE and future missions* (pp. 123–129), Springer: Berlin.

Bruinsma, S., & Biancale, R. (2003). Total densities derived from accelerometer data. *Journal of Spacecraft and Rockets*, *40*(2), 230–236.

Bruinsma, S., Forbes, J. M., Nerem, R. S., & Zhang, X. (2006). Thermosphere density response to the 20–21 November 2003 solar and geomagnetic storm from CHAMP and GRACE accelerometer data. *Journal of Geophysical Research*, *111*, A06303. https://doi.org/10.1029/2005JA011284

Bruinsma, S., Doornbos, E., & Bowman, B. (2014). Validation of GOCE densities and evaluation of thermosphere models. *Advances in Space Research*, *54*(4), 576–585.

Doornbos, E., Den Ijssel, J. V., Lühr, H., Förster, M., & Koppenwallner, G. (2010). Neutral density and crosswind determination from arbitrarily oriented multiaxis accelerometers on satellites. *Journal of Spacecraft and Rockets*, *47*(4), 580–589.

Doornbos, E., Bruinsma, S., Fritsche, B., Visser, P., Van Den IJssel, J., Encarnacao, J. T., & Kern, M. (Eds.). (2013). Air density and wind retrieval using GOCE data. *ESA Living Planet Symposium, Proceedings of the conference held on 9–13 September 2013 at Edinburgh in United Kingdom* (p. 7), ESA SP-722. 2–13: TU Delft, Netherlands.

Doornbos, E., Bruinsma, S., Fritsche, B., Koppenwallner, G., Visser, P., van den IJssel, J., & de Encarnação, J. D. T. (2014). GOCE+ Theme 3: Air density and wind retrieval using GOCE data (Final Rep.), TU Delft, Netherlands.

Drinkwater, M. R., Haagmans, R., Muzi, D., Popescu, A., Floberghagen, R., Kern, M., & Fehringer, M. (2006). The GOCE gravity mission: ESAs first core Earth explorer (Proceedings of the 3rd international GOCE user workshop (pp. 6–8), European Space Agency Noordwijk: The Netherlands.

Drob, D. P., Emmert, J. T., Meriwether, J. W., Makela, J. J., Doornbos, E., Conde, M., … Klenzing, J. H. (2015). An update to the horizontal wind model (HWM): The quiet time thermosphere. *Earth and Space Science*, *2*(7), 301–319.

ESA, S. C. (2006). GOCE l1b products user handbook (Tech. Rep.), The European GOCE Gravity Consortium EGG-GOCE-GSEG-EOPG-TN-06-0137.

Feynman, R., Leighton, R., & Sands, M. (Eds.). (1964). *The Feynman lectures on physics* (pp. 41–1). Reading, MA: Addison–Wesley.

Floberghagen, R., Fehringer, M., Lamarre, D., Muzi, D., Frommknecht, B., … Da Costa, A. (2011). Mission design, operation and exploitation of the gravity field and steady-state ocean circulation explorer mission. *Journal of Geodesy*, *85*(11), 749–758.

Forbes, J. M., Lu, G., Bruinsma, S., Nerem, S., & Zhang, X. (2005). Thermosphere density variations due to the 15–24 April 2002 solar events from CHAMP/STAR accelerometer measurements. *Journal of Geophysical Research*, *110*, A12S27. https://doi.org/10.1029/2004JA010856

Förster, M., Rentz, S., Köhler, W., Liu, H., & Haaland, S. (2008). IMF dependence of high-latitude thermospheric wind pattern derived from CHAMP cross-track measurements. *Annales Geophysicae*, *26*, 1581–1595.

Fremouw, E., Carlson, H., Potemra, T., Bythrow, P., Rino, C., Vickrey, J., … Livingston, R. L. (1985). The HILAT satellite mission. *Radio Science*, *20*(3), 416–424.

Frommknecht, B., Lamarre, D., Meloni, M., Bigazzi, A., & Floberghagen, R. (2011). GOCE level 1b data processing. *Journal of Geodesy*, *85*(11), 759–775.

Garcia, R. F., Bruinsma, S., Massarweh, L., & Doornbos, E. (2016). Medium-scale gravity wave activity in the thermosphere inferred from GOCE data. *Journal of Geophysical Research: Space Physics*, *121*, 8089–8102. https://doi.org/10.1002/2016JA022797

Gasperini, F., Forbes, J., Doornbos, E., & Bruinsma, S. (2015). Wave coupling between the lower and middle thermosphere as viewed from TIMED and GOCE. *Journal of Geophysical Research: Space Physics*, *120*, 5788–5804. https://doi.org/10.1002/2015JA021300

Huang, C. Y.-Y., Huang, Y., Su, Y.-J., Sutton, E. K., Hairston, M. R., & Coley, W. R. (2016). Ionosphere-thermosphere (IT) response to solar wind forcing during magnetic storms. *Journal of Space Weather and Space Climate*, *6*, A4.

Ince, E. S., & Pagiatakis, S. D. (2015). Effects of the magnetic field on the GOCE level 1b gradiometer data over magnetic poles. In L. Ouwehand (Eds.) *Proceedings of the 5th International GOCE User Workshop* (Vol. 728, p. 29), Paris, France: ESA-SP.

Ince, E. S., & Pagiatakis, S. D. (2016). Effects of space weather on GOCE electrostatic gravity gradiometer measurements. *Journal of Geodesy*, *90*(12), 1389–1403.

Kelley, M., Knudsen, D., & Vickrey, J. (1991). Poynting flux measurements on a satellite: A diagnostic tool for space research. *Journal of Geophysical Research*, *96*(A1), 201–207.

Kelley, M. C. (2009). The Earth's Ionosphere: Plasma Physics and Electrodynamics, (2nd ed.), by Michael C. Kelly. San Diego, CA: Academic Press (Elsevier). ISBN 978-0-12-088425-4.
Killeen, T., & Roble, R. (1988). Thermosphere dynamics: Contributions from the first 5 years of the dynamics explorer program. *Reviews of Geophysics*, *26*(2), 329–367. https://doi.org/10.1029/90JA01837
Knipp, D., Eriksson, S., Kilcommons, L., Crowley, G., Lei, J., Hairston, M., & Drake, K. (2011). Extreme Poynting flux in the dayside thermosphere: Examples and statistics. *Geophysical Research Letters*, *38*, L16102. https://doi.org/10.1029/2011GL048302
Knudsen, D., Burchill, J., Buchert, S., Eriksson, A., Gill, R., & Wahlund, J.-E. (2017). Thermal ion imagers and Langmuir probes in the SWARM electric field instruments. *Journal of Geophysical Research: Space Physics*, *122*, 2655–2673. https://doi.org/10.1002/2016JA022571
Kwak, Y.-S., & Richmond, A. (2007). An analysis of the momentum forcing in the high-latitude lower thermosphere. *Journal of Geophysical Research*, *112*, A01306. https://doi.org/10.1029/2006JA011910
Lennart, L. (1999). *System identification: Theory for the user* (pp. 1–14). Upper Saddle River, NJ: PTR Prentice Hall.
Liu, H., Doornbos, E., & Nakashima, J. (2016). Thermospheric wind observed by GOCE: Wind jets and seasonal variations. *Journal of Geophysical Research: Space Physics*, *121*, 6901–6913. https://doi.org/10.1002/2016JA022938
Lu, G., Hagan, M., Häusler, K., Doornbos, E., Bruinsma, S., Anderson, B., & Korth, H. (2014). Global ionospheric and thermospheric response to the 5 April 2010 geomagnetic storm: An integrated data-model investigation. *Journal of Geophysical Research: Space Physics*, *119*, 10,358–10,375. https://doi.org/10.1002/2014JA020555
Lühr, H., Rother, M., Köhler, W., Ritter, P., & Grunwaldt, L. (2004). Thermospheric up-welling in the cusp region: Evidence from CHAMP observations. *Geophysical Research Letters*, *31*, L06805. https://doi.org/10.1029/2003GL019314
Lühr, H., Rentz, S., Ritter, P., Liu, H., & Häusler, K. (2007). *Average thermospheric wind patterns over the polar regions, as observed by CHAMP* (vol. 25, pp. 1093–1101).
Mayer-Gürr, T., Zehentner, N., Klinger, B., & Kvas, A. (2014). ITSG-grace2014: A new GRACE gravity field release computed in Graz. *Presentation at the GRACE Science Team Meeting (GSTM)* (Vol. 9), Potsdam, Germany.
Peterseim, N., Schlicht, A., Stummer, C., & Yi, W. (2011). Impact of cross winds in polar regions on GOCE accelerometer and gradiometer data (Proceedings of the 4th International GOCE User Workshop (Vol. 31)), Noordwijk, Netherlands: European Space Agency.
Roble, R. (1996). The near thermosphere-ionosphere-mesosphere-electrodynamics general circulation model (TIME-GCM) *STEP Handbook on Ionospheric Models* (pp. 281–288), Logan: Utah State University.
Rummel, R., Yi, W., & Stummer, C. (2011). GOCE gravitational gradiometry. *Journal of Geodesy*, *85*(11), 777–790.
Siemes, C. (2012). GOCE gradiometer calibration and level 1b data processing. (Tech. Rep.), Noordwijk, Netherlands: ESA Working Paper EWP-2384. https://doi.org/https://earth.esa.int/c/document_library/get_file
Siemes, C. (2017). Improving GOCE cross-track gravity gradients. *Journal of Geodesy*, 1–13. https://doi.org/10.1007/s00190-017-1042-x
Siemes, C., Haagmans, R., Kern, M., Plank, G., & Floberghagen, R. (2012). Monitoring GOCE gradiometer calibration parameters using accelerometer and star sensor data: Methodology and first results. *Journal of Geodesy*, *86*(8), 629–645.
Stolle, C., Floberghagen, R., Lühr, H., Maus, S., Knudsen, D., Alken, P., … Visser, P. N. (2013). Space weather opportunities from the SWARM mission including near real time applications. *Earth, Planets and Space*, *65*(11), 1375–1383.
Stummer, C., Siemes, C., Pail, R., Frommknecht, B., & Floberghagen, R. (2012). Upgrade of the GOCE level 1b gradiometer processor. *Advances in Space Research*, *49*(4), 739–752.
Sutton, E. K., Nerem, R. S., & Forbes, J. M. (2007). Density and winds in the thermosphere deduced from accelerometer data. *Journal of Spacecraft and Rockets*, *44*(6), 1210–1219.
Thayer, J. P., & Killeen, T. (1993). A kinematic analysis of the high-latitude thermospheric neutral circulation pattern. *Journal of Geophysical Research*, *98*(A7), 11,549–11,565.
Untiedt, J., & Baumjohann, W. (1993). Studies of polar current systems using the IMS Scandinavian magnetometer array. *Space Science Reviews*, *63*(3–4), 245–390.
Weygand, J., & Wing, S. (2016). Comparison of DMSP and SECS region-1 and region-2 ionospheric current boundary. *Journal of Atmospheric and Solar-Terrestrial Physics*, *143*, 8–13.
Weygand, J. M., Amm, O., Viljanen, A., Angelopoulos, V., Murr, D., Engebretson, M., … Mann, I. (2011). Application and validation of the spherical elementary currents systems technique for deriving ionospheric equivalent currents with the North American and Greenland ground magnetometer arrays. *Journal of Geophysical Research*, *116*, A03305. https://doi.org/10.1029/2010JA016177
Zhang, J., Wang, C., Tang, B., & Li, H. (2013). Effect of the solar wind conditions on the ionospheric equivalent current systems. *Annales Geophysicae*, *31*, 489–501.